文章编号：1001-9014(2023)04-0468-08

DOI:10.11972/j.issn.1001-9014.2023.04.007

Wavelength extended InGaAsBi near infrared photodetector

FENG Duo, DAI Jin-Meng, CAO You-Xiang, ZHANG Li-Yao*

(Department of Physics, University of Shanghai for Science and Technology, Shanghai 200093, China)

Abstract: InGaAs photodetector is widely used in SWIR detection. Bi incorporation into InGaAs can reduce the bandgap, extending the detection wavelength. By controlling of the In and Bi compositions, the detection wavelength could be extended to over 3 μm from $In_yGa_{1-y}As_{1-x}Bi_x$, lattice-matched to InP. An $In_{0.394}Ga_{0.606}As_{0.913}Bi_{0.087}$ p-i-n photodetector is designed and its performance is numerically investigated. Dark currents and responsivity spectra are calculated with different temperatures, absorption layer thicknesses and doping concentrations. A 50% cut-off wavelength of 3 μm is achieved. The proposed structure provides a feasible way to fabricate InGaAsBi based SWIR detector with longer detection wavelength.

Key words: InGaAsBi, dark current, responsivity, SWIR

波长拓展型InGaAsBi近红外探测器

冯 铎, 代金梦, 曹有祥, 张立瑶*

(上海理工大学 物理系, 上海 200093)

摘要:InGaAs光电探测器广泛应用于短波红外检测。在InGaAs中掺入Bi可以减小带隙,延长探测波长。通过控制In和Bi的组分可使$In_yGa_{1-y}As_{1-x}Bi_x$与InP晶格匹配,同时,扩展探测波长至3 μm以上。设计并研究了$In_{0.394}Ga_{0.606}As_{0.913}Bi_{0.087}$ p-i-n光电探测器的光电性能。计算了不同温度、吸收层厚度和p(n)区掺杂浓度下的暗电流和响应率特性。获得了3 μm的截止波长。该结构为拓展InP基晶格匹配的短波红外探测器的探测波长提供了一种可行的方法。

关 键 词:铟镓砷铋;暗电流;响应率;短波红外

中图分类号:TN215 **文献标识码**:A

Introduction

Short-wave infrared (SWIR) detectors have been widely used in night vision, optical fiber communications and environmental monitoring, etc[1]. Because of the high optical absorption coefficient and carrier mobility, InGaAs shows good performance in SWIR detection at room temperature. The cutoff wavelength of $In_{0.53}Ga_{0.47}As$ detectors, lattice-matched to InP is 1.7 μm. The In composition is further increased in InGaAs to extend detection wavelengths, however, high In content introduces lattice mismatch, thus deteriorates the device performances[2,3]. Many efforts have been made to compensate the lattice mismatch, such as introducing $In_xAl_{1-x}As$ graded buffer layers between InGaAs and InP substrate[4-7] and using $In_{0.66}Ga_{0.34}As$/InAs superlattices[8]. Whereas, the device performance is still nonideal, comparing to the performance of the device fabricated with strain-free InGaAs.

Dilute bismides, which are formed by incorporating a small quantity of Bi atoms into the traditional group III-V compound semiconductors, have attracted wide attentions[9-10]. The isoelectronic energy level of Bi lies in the valence bands (VB) of most III-Vs[11], which results in the VB anti-crossing in dilute bismides, thus reducing the bandgap of dilute bismides. Moreover, Bi incorporation could increase the spin-orbit splitting energy and suppress Auger recombination[12]. The bandgap reduction of InGaAsBi is about 56 meV/Bi%[13], which is from the VB upshift[14]. In incorporation into InGaAs offers a bandgap reduction of 10 meV/In%[12]. InGaAsBi can be lattice matched to InP by controlling the In and Bi con-

Received date: 2023-02-02, **revised date**: 2023-04-12 **收稿日期**:2023-02-02,**修回日期**:2023-04-12

Foundation items: Supported by the National Natural Science Foundation of China (61904106)

Biography: FENG Duo (1997-), male, Yangquan, master. Research area involves III-V Photoelectronic materials and devices. E-mail: 202232249@st.usst.edu.cn.

* **Corresponding author**: E-mail: lyzhang@usst.edu.cn

tents. Also, the detection wavelength of InGaAsBi could reach and exceed 3 μm with proper In and Bi contents. Till now, the highest Bi content in InGaAsBi is 7.5%[15]. Strong photoluminescence spectra were achieved from both InGaAsBi thin films[16] and QWs[17]. An $In_{0.76}GaAsBi_{0.027}$ photodetector on InP with a 50% cutoff wavelength of 2.63 μm at RT was demonstrated in 2018[18]. $In_{0.47}GaAsBi_{0.07}$/InAlAs single quantum well with an emission wavelength of 2.5 μm was realized in 2020[19]. Good electrical and optical properties make InGaAsBi a potential material for fabricating optoelectronic devices.

In this work, we proposed an $In_yGa_{1-y}As_{1-x}Bi_x$ photodetector which is lattice matched to InP substrate by adjusting x and y. Dark currents and responsivities of the InGaAsBi detector were investigated theoretically. With the proposed structure, a cutoff wavelength at 3 μm was achieved.

1 Method

According to Vegard's law, the lattice constant of the quaternary alloy $In_yGa_{1-y}As_{1-x}Bi_x$ is

$$a_{InGaAsBi} = (1-x)(1-y)a_{InAs} + x(1-y)a_{InBi} + (1-x)ya_{GaAs} + xya_{GaBi} \quad , \quad (1)$$

$In_yGa_{1-y}As_{1-x}Bi_x$ is lattice matched to InP when y=0.53-1.56x[12]. Because the bandgap reductions of $In_yGa_{1-y}As_{1-x}Bi_x$ are 56 meV/Bi% and 10 meV/In%, the bandgap of $In_yGa_{1-y}As_{1-x}Bi_x$ lattice-matched to InP is

$$E_g = 1.0465x^2 - 3.9867x + 0.7511 \quad . \quad (2)$$

When the Bi content is over 8.7%, the bandgap of $In_yGa_{1-y}As_{1-x}Bi_x$ is below 0.41 eV, thus the theoretical cutoff wavelength exceeds 3 μm. $In_{0.394}Ga_{0.606}As_{0.913}Bi_{0.087}$ is proposed to fabricate SWIR detector, with detection wavelength extended to 3 μm.

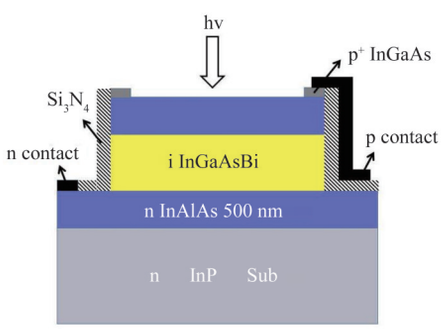

Fig. 1　The schematic structure of the $In_{0.394}Ga_{0.606}As_{0.913}Bi_{0.087}$/$In_{0.52}Al_{0.48}As$ p-i-n photodetector

图 1　$In_{0.394}Ga_{0.606}As_{0.913}Bi_{0.087}$/$In_{0.52}Al_{0.48}As$ p-i-n 光电探测器的结构示意图

Figure 1 shows the schematic structure of the proposed $In_{0.394}Ga_{0.606}As_{0.913}Bi_{0.087}$ p-i-n detector. The device performance is simulated using the finite element method by Comsol Multiphysics.

The potential and carrier distributions are calculated by solving Poisson's equation and continuity equations:

$$\nabla^2\psi = -\frac{\rho}{\varepsilon} \quad , \quad (3)$$

$$\frac{\partial n}{\partial t} = \frac{1}{q}\nabla\cdot J_n + (G_{rad} - R_{SRH}) \quad , \quad (4)$$

$$\frac{\partial p}{\partial t} = \frac{1}{q}\nabla\cdot J_p + (G_{rad} - R_{SRH}) \quad , \quad (5)$$

where ψ is the electrostatic potential, ε is the dielectric constant, q is the charge density, $n(p)$ is the electron (hole) concentration, $J_{n(p)}$ is the electron (hole) current density, G_{rad} is the photogeneration rate, and R_{SRH} is the Shockley-Read-Hall (SRH) recombination rate. The photogeneration rate G_{rad} is [20]

$$G_{rad} = Q(1-r)\alpha e^{-\alpha d} \quad , \quad (6)$$

where Q is the incident photon flux, r is the reflectivity, α is the absorption coefficient, d is the distance from the surface of the detector. The absorption coefficient α is deduced from the absorption spectra in Ref. 16[16].

The SRH recombination rate is

$$R_{SRH} = \frac{np - \gamma_n\gamma_p n_i^2}{\tau_p\left(n + \gamma_n n_i \exp\left(\frac{E_t - E_f}{kT}\right)\right) + \tau_n\left(p + \gamma_p n_i \exp\left(\frac{E_t - E_f}{kT}\right)\right)} \quad , \quad (7)$$

$$n_i = \sqrt{N_C N_V}\exp\left(-\frac{E_g}{2kT}\right) \quad , \quad (8)$$

where τ_p and τ_n are the hole and electron lifetimes due to SRH processes, γ_n and γ_p are proportionality factors of electron and holes separately, n_i and E_f are the intrinsic carrier concentration and intrinsic Fermi level, E_t is recombination central level.

2 Results and Discussion

Dark current is an important parameter for evaluating the performance of a detector. For p-i-n detectors, dark current densities mainly consist of diffusion current densities (J_{diff}), generation-recombination current densities (J_{GR}), the Trap assisted tunneling current densities (J_{TAT}) and Band-to-band tunneling current densities (J_{BTB}) [21-23].

$$J_{diff} = n_i^2\sqrt{qkT}\left(\frac{1}{N_A}\sqrt{\frac{\mu_n}{\tau_n}} + \frac{1}{N_D}\sqrt{\frac{\mu_p}{\tau_p}}\right)\left[\exp\left(\frac{qV}{kT}\right) - 1\right] \propto \exp\left(-\frac{E_g}{kT}\right)\left[\exp\left(\frac{qV}{kT}\right) - 1\right] \quad , (9)$$

$$J_{GR} = \frac{n_i}{\tau_{GR}}\sqrt{\frac{q\varepsilon_0\varepsilon_r V_t(N_A + N_D)}{2N_A N_D}}\left[\exp\left(\frac{qV}{2kT}\right) - 1\right] \propto \exp\left(-\frac{E_g}{2kT}\right)\left[\exp\left(\frac{qV}{2kT}\right) - 1\right] \quad , \quad (10)$$

$$J_{TAT} = \frac{m_T N_T V(qM)^2}{8\pi\hbar^3(E_g - E_t)}\exp\left\{-\frac{4\sqrt{2m_T(E_g - E_t)^3}}{3Eq\hbar}\right\} \quad , (11)$$

$$J_{BTB} = \frac{q^3 EV}{4\pi^2\hbar^2}\sqrt{\frac{2m_e}{E_g}}\exp\left(-\frac{4\sqrt{2m_e E_g^3}}{3Eq\hbar}\right) \quad , \quad (12)$$

where $\mu_{n(p)}$ is the mobility of electrons (holes), N_A and N_D are the doping concentrations of acceptors and donors, respectively. V is the bias voltage, τ_{GR} is the generation-combination lifetime, ε_r and ε_0 are the relative effective

dielectric constant and permittivity of free space, $V_t = V_d - V$ is the total junction potential, V_d is the built-in potential, m_T is the reduced tunneling effective mass, the trap energy level E_t is close to the middle of effective band gap ($0.51E_g$) according to Chen, et al[24]. M^2 is the matrix elements associated with trap potential. E is the maximum junction electric field. N_T is the activated trap density.

At low biases, Eq. (9) and Eq. (10) could be represented by

$$J \propto \exp(-E_a/kT) \quad , \quad (13)$$

where E_a is the thermal activation energy, extracted from fitting the I–V curve. The dark current is dominated by the diffusion current while $E_a \approx E_g$, and dominated by the generation-recombination current while $E_a \approx E_g/2$. The parameters used for the calculations are summarized in Table 1.

Table 1 Parameters used in this calculation

表1 本计算中所使用的参数

Parameters	Units	$In_{0.394}Ga_{0.606}As_{0.913}Bi_{0.087}$
m_e	(kg)	0.043 m_0[25]
m_{hh}	(kg)	0.130 54 m_0[25]
m_{lh}	(kg)	0.053 14 m_0[26]
m_T	(kg)	0.032 4 m_0
ε_r	1	13.88[27]
τ_p	(s)	1e-12[28]
τ_n	(s)	3e-12[28]
τ_{GR}	(s)	1e-8[29]
μ_p	($cm^2/(V\cdot s)$)	1 000[28]
μ_n	($cm^2/(V\cdot s)$)	3 000[29]
ε_r	1	13.88[27]
N_T	(m^{-3})	2e-5[28]
E_t	(eV)	$0.51E_g$[24]
M^2	(eV^2cm^3)	1e-23[24]

The performances of the InGaAsBi p-i-n detectors are investigated with different temperatures and thicknesses of InGaAsBi and doping concentrations of both InAlAs and InGaAsBi.

2.1 Temperature

Figure 2(a) shows the variation of dark currents with temperatures. Dark current densities decrease with the decrease of temperatures. Under a reverse bias of -10 mV, the dark current densities are about 1.32×10^{-2} A/cm^2 at RT and 2.09×10^{-13} A/cm^2 at 77 K.

Trap-assisted tunneling (TAT) and Band-to-band tunneling (BTB) currents are both negligible at low bias and significantly increase with the bias, which is associated with the field enhancement leakage process as Trap-assisted tunneling and Band-to-band tunneling. The tunneling carriers may bridge the forbidden gap directly and give rise to BTB current. The TAT and BTB I–V characteristics are simulated at large reverse biases (-10~-2 V) and shown in Figs. 2(c) and (d), respectively. It can

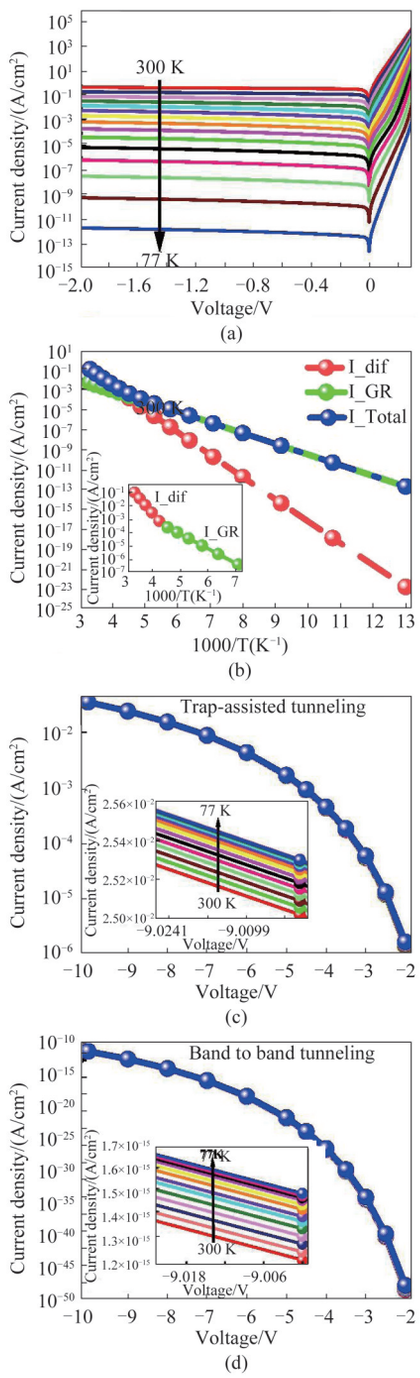

Fig. 2 Dark I-V curves (a), total dark currents, diffusion and generation-recombination currents versus 1 000/T (b), trap-assisted tunneling current I-V curves (c) and Band-to-band direct tunneling current I-V curves (d) at different temperatures of InGaAsBi detectors. The thickness of InGaAsBi is 1.5 μm and the doping concentration is 5×10^{15} cm^{-3}, the doping concentration of InAlAs is 1×10^{18} cm^{-3}. The temperature increases from 77 K to 300 K

图2 InGaAsBi探测器:(a)不同温度下的暗电流-电压曲线,(b)暗电流、扩散电流和产生-复合电流随1 000/T的变化,(c)不同温度下的缺陷辅助隧穿电流-电压曲线,(d)不同温度下的带间直接隧穿电流-电压曲线。其中,InGaAsBi探测器中,InGaAsBi的厚度为1.5 μm,掺杂浓度为5×10^{15} cm^{-3},InAlAs的掺杂浓度为1×10^{18} cm^{-3}。温度变化范围为从77 K到300 K

be seen that both the TAT and BTB currents are independent of the temperature. Because the InGaAsBi photodetector usually works under low bias, the TAT and BTB currents are negligible. Only the diffusion and generation-recombination currents are discussed in the following sections. Arrhenius plots of dark current densities against 1 000/T are shown in Fig. 2(b). The dark current densities decrease exponentially with 1 000/T. The thermal activation energy E_a is fitted from the I–V curves. When the temperature is above 240 K, the fitted E_a is about 0.4 eV, close to the bandgap of InGaAsBi, the detector is dominated by the diffusion current from 240 K to 300 K. When the temperature is below 240 K, the fitted E_a is about 0.2 eV, close to half the bandgap of InGaAsBi, informing that the generation-recombination current is dominant at the small reverse bias.

The normalized responsivities of InGaAsBi detectors at different temperatures are discussed under a reverse bias of -10 mV. The InGaAsBi p-i-n detectors are with a 1.5 μm-thick InGaAsBi layer and a doping concentration of 5×10^{15} cm^{-3}, and InAlAs layers with doping concentrations of 1×10^{18}cm^{-3}. As shown in Fig. 3(a), the responsivities reach maximum at around 2.4 μm, and the 50% cutoff wavelength is about 3 μm. The variation of the responsivities under different incident wavelength with temperatures is shown in Fig. 3(b). The responsivities are almost unchanged with the temperature.

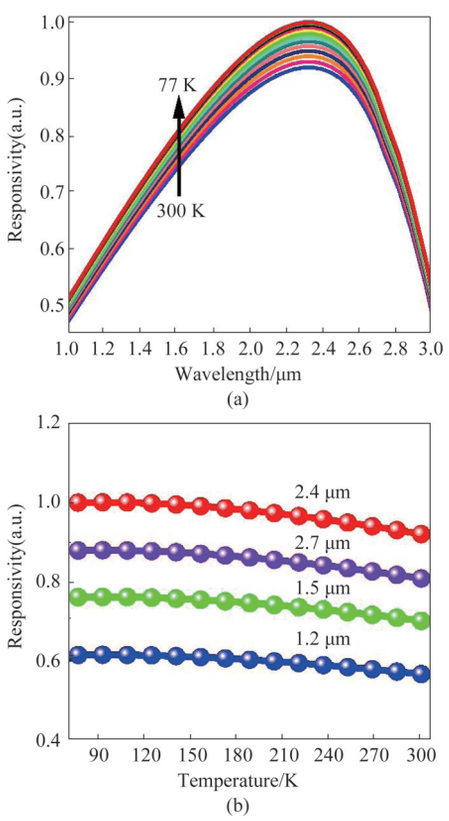

Fig. 3　(a) Normalized responsivity spectra of the InGaAsBi p-i-n detector under different temperatures, (b) responsivities versus T at different incident wavelengths. The responsivities' spectra are calculated under a bias of -10 mV, from InGaAsBi detectors with the 1.5-μm-thick absorption layers, the doping concentrations of 1×10^{18} cm^{-3} in InAlAs layers and 5×10^{15} cm^{-3} in InGaAsBi layers, respectively

图 3　InGaAsBi p-i-n 探测器:(a)在不同温度下的归一化响应率谱,(b)不同入射波长下响应度随温度的变化曲线,拟合条件为:在-10 mV 偏压下,吸收层厚度为 1.5 μm,InAlAs 层和 InGaAsBi 层的掺杂浓度分别为 1×10^{18} cm^{-3} 和 5×10^{15} cm^{-3}

2.2　Thickness

Dark current densities of InGaAsBi detectors with different absorption layer thicknesses are further discussed and shown in Fig. 4. The dark current densities are calculated under a bias of -10 mV at 300 K, and the doping concentrations of the InAlAs layers are 1×10^{18} cm^{-3}. The thicknesses of InGaAsBi increase from 0.1 μm to 3.0 μm. As shown in Fig. 4(a), the effect of the thicknesses of InGaAsBi on dark current densities is subtle under low reverse bias and increases with the reverse bias. Figure 4(b) shows the relationship between dark current densities and the thicknesses of InGaAsBi.

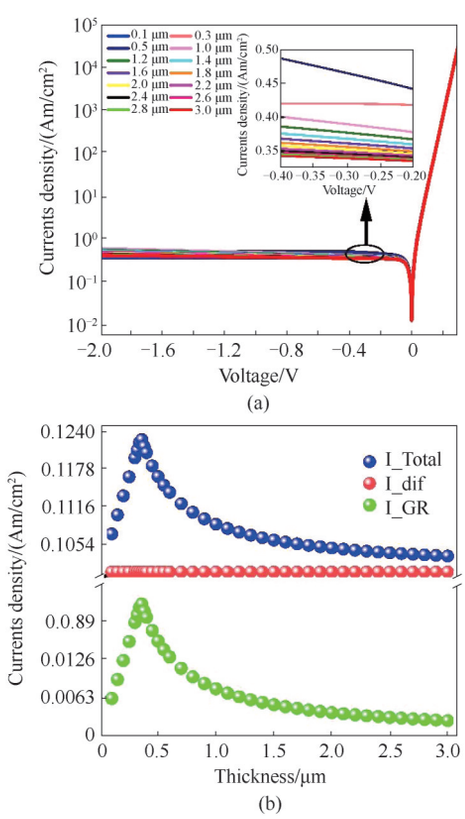

Fig. 4　Dark I-V curves with different thicknesses of the absorption layer (a) and total dark currents, diffusion and generation-recombination currents versus the thickness of the absorption layer under -10 mV(b) of InGaAsBi detectors. The dark current characteristics are simulated at 300 K. The doping concentration of InAlAs and InGaAsBi are 1×10^{18} cm^{-3} and 5×10^{15} cm^{-3}, respectively

图 4　不同吸收层厚度的 InGaAsBi 探测器的:(a)暗电流-电压曲线,(b) -10 mV 下总暗电流、扩散电流和产生复合电流随吸收层厚度的变化关系。其中,拟合温度为 300 K,InAlAs 和 InGaAsBi 的掺杂浓度分别为 1×10^{18} cm^{-3} 和 5×10^{15} cm^{-3}

The dark current densities increase with the thicknesses of InGaAsBi increasing from 0.1 μm to 0.36 μm, where the InGaAsBi layer is completely depleted, and decrease to a stable value with the thicknesses further increasing. As shown in Eq. (9), the diffusion current is insensitive to the thicknesses of absorption layer, while the generation-recombination current is proportional to the depletion width. When the absorption layer thickness is small, the InGaAsBi layer is completely depleted, thus the generation-recombination current increases with the thickness of InGaAsBi. However, with the thickness of InGaAsBi above 0.36 μm, the InGaAsBi layer is partially depleted and the depletion width would decrease with the thickness of InGaAsBi, thus the generation-recombination current decreases.

The influences of the absorption layer thicknesses on responsivity are calculated and shown in Fig. 5. The variation of the responsivity with the thickness of the absorption layer is determined by diffusion and absorption[30]. When the absorption layer is thin, the absorption is dominant, thus the responsivity increases with the thickness of the absorption layer. When the absorption layer is thick enough, the diffusion is dominant, thus the responsivity decreases with the absorption layer thickness.

2.3 Doping concentration

Figure 6 shows the dark current characteristics of InGaAsBi detectors with different doping concentrations of InAlAs layers. As shown in Fig. 6(a), the influence of the doping concentrations on the dark current density is subtle under large reverse bias. The variations of total dark current, diffusion and generation-recombination currents under -10 mV with the doping concentrations are shown in Fig. 6(b). The diffusion current decreases while the generation-recombination current increases with the doping concentrations. Because the diffusion current is dominant, the total dark current decreases with the doping concentrations.

Figure 7 shows the responsivities of the detectors calculated at 300 K under a bias of -10 mV. The doping concentrations of InAlAs vary from 5.0×10^{17} cm^{-3} to 1.0×10^{19} cm^{-3}, resulting in a depletion width variation from 76.5 nm to 108.1 nm. As shown in Fig. 7(b), the responsivities significantly increase with the doping concentrations of InAlAs increasing to 2.0×10^{18} cm^{-3}, and then slightly increase with the doping concentrations further increasing.

Figure 8 shows the *I-V* characteristics under different doping concentrations of the absorption layer. The thickness of InGaAsBi is 1.5 μm, under which the InGaAsBi layer is partially depleted with the doping concentration varies from 1×10^{15} cm^{-3} to 5×10^{16} cm^{-3}. The generation-recombination current decreases with the doping concentration in InGaAsBi, while the diffusion current hardly changes. With the doping concentration in InGaAsBi increasing from 1×10^{15} cm^{-3} to 1×10^{16} cm^{-3}, the depletion width decreases from 419 nm to 41.9 nm, thus the generation-recombination current significantly decreases. When the doping concentration increases to 3×10^{16} cm^{-3}, the depletion width decreases to 14 nm, causing a slowly decreasing of generation-recombination current. With the doping concentration continuously increasing, the depletion width is extremely thin, resulting in a low generation-recombination current, that hardly influences the total current.

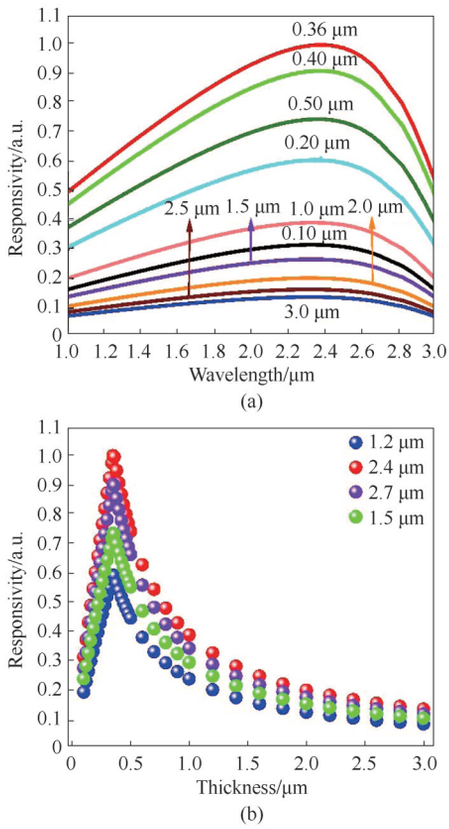

Fig. 5 Normalized responsivity spectra (a) and responsivities at different incident wavelengths (b) with different absorption layer thicknesses. The responsivities are calculated under a bias of -10 mV at 300 K. The doping concentration of InAlAs and InGaAsBi are 1×10^{18} cm^{-3} and 5×10^{15} cm^{-3}, respectively

图5 (a) 不同吸收层厚度的归一化响应谱,(b)不同入射波长下,响应率随吸收层厚度的变化,其中,响应率在300 K时,-10 mV下计算得到,InAlAs和InGaAsBi的掺杂浓度分别为1×10^{18} cm^{-3}和5×10^{15} cm^{-3}

Figure 9 shows the responsivities of InGaAsBi detectors with 1.5-μm-thick absorption layers are calculated at 300 K under a bias of -10 mV. As shown in Fig. 9(a), the responsivities decrease with the doping concentrations of InGaAsBi layers.

The quantum efficiency is exponential to the depletion width[31], thus when the doping concentration increases from 1.0×10^{15} cm^{-3} to 1.0×10^{16} cm^{-3}, the responsivity significantly decreases, as shown in Fig. 9(b). With the doping concentration continuously increasing, the responsivity slightly decreases.

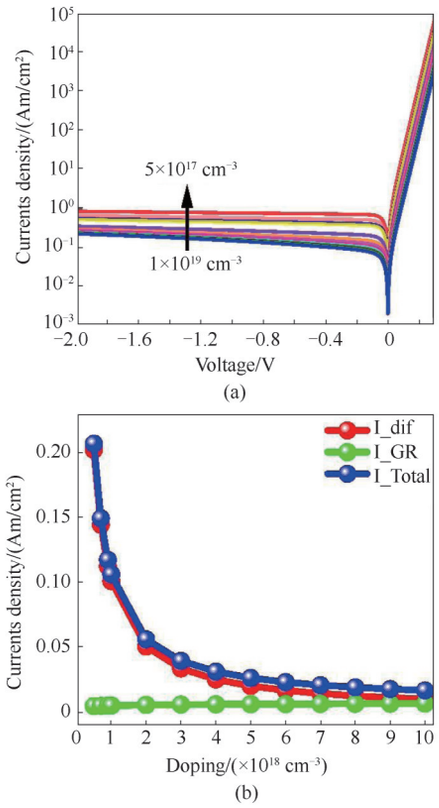

Fig. 6　Dark *I-V* curves (a) and total dark currents, diffusion and generation-recombination currents at a bias of -10 mV (b) of InGaAsBi detectors with different doping concentrations of InAlAs layers. The dark current characteristics are simulated at 300 K. The thickness and doping concentration of InGaAsBi are 1.5 μm and 5×10^{15} cm^{-3}, respectively

图 6　不同 InAlAs 掺杂浓度下，InGaAsBi 探测器(a)暗电流-电压曲线，(b) -10 mV 偏压下，总暗电流、扩散电流和产生复合电流随 InAlAs 掺杂浓度的变化曲线，其中，拟合温度为 300 K，InGaAsBi 的厚度为 1.5 μm，掺杂浓度为 5×10^{15} cm^{-3}

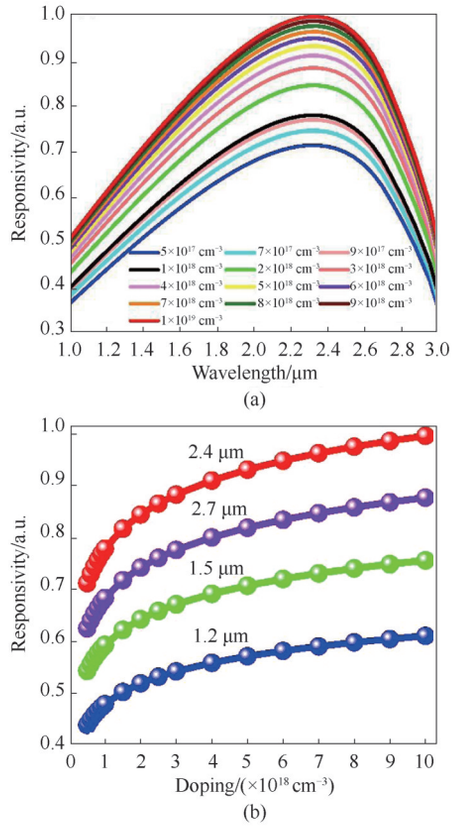

Fig. 7　Normalized responsivity spectra (a) and responsivities under different incident wavelengths (b) of InGaAsBi detectors with different doping concentrations of InAlAs. The responsivities are calculated under a bias of -10 mV at 300 K. The thickness and doping concentration of InGaAsBi are 1.5 μm and 5×10^{15} cm^{-3}, respectively

图 7　InGaAsBi 探测器：(a)归一化响应谱，(b)不同入射光波长下响应率随 InAlAs 掺杂浓度的变化曲线，其中，InGaAsBi 的厚度为 1.5 μm，掺杂浓度为 5×10^{15} cm^{-3}，拟合温度为 300 K，偏置电压为-10 mV

3　Conclusion

In this paper, an $In_{0.394}Ga_{0.606}As_{0.913}Bi_{0.087}$ p-i-n photodetector, lattice-matched to InP, is proposed to extend the detection wavelength. The dark current and responsivity are calculated with different temperatures, absorption layer thicknesses and doping concentrations. Dark currents increase with temperatures. The diffusion current is dominant when the temperature is above 240 K, while the generation-recombination current is dominant when the temperature is below 240 K. The influence of temperature on the responsivity is subtle. Dark currents increase with the absorption layer thickness when the absorption layer is completely depleted, and decrease with the absorption layer thickness when the absorption layer is partially depleted. A similar trend is found in the responsivity. Dark currents decrease with the doping concentrations in both InAlAs and InGaAsBi, but the responsivities are of the opposite trend. These results provide a feasible way to extend the detection wavelength in SWIR detectors.

References

[1] Zhang Y G, Gu Y, Wang K, *et al*. Properties of gas source molecular beam epitaxy grown wavelength extended InGaAs photodetector structures on a linear graded InAlAs buffer [J]. *Semiconductor Science and Technology*, 2008. **23**(12).

[2] Zhang Y G, Gu Y, Tian Z B, *et al*. Wavelength extended InGaAs/InAlAs/InP photodetectors using n-on-p configuration optimized for back illumination [J]. *Infrared Physics & Technology*, 2009. **52**(1): 52-56.

[3] Gu Y, Zhang Y G, Ma Y J, *et al*. InP-based type-I quantum well lasers up to 2.9 μm at 230 K in pulsed mode on a metamorphic buffer [J]. *Applied Physics Letters*, 2015. **106**(12).

[4] Andresen B F, Yuan H, Fulop G F, *et al*. FPA development: from InGaAs, InSb, to HgCdTe [J]. *Infrared Technology and Applications XXXIV*, 2008.

[5] Gu Y, Wang K, Li C, *et al*. High indium content InGaAs photodetector: with InGaAs or InAlAs graded buffer layers [J]. *Journal of Infrared and Millimeter Waves*, 2012. **30**(6): 481-485.

[6] Chyi J I, Shieh J L, Pan J W, *et al*. Material properties of compositional graded $In_xGa_{1-x}As$ and $In_xAl_{1-x}As$ epilayers grown on GaAs sub-

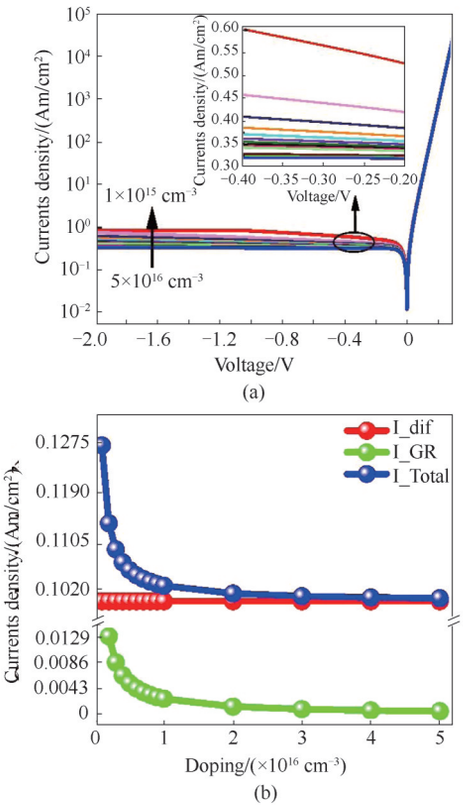

Fig. 8 Dark *I-V* curves (a) and total dark currents, diffusion and GR currents at a bias of -10 mV (b) of InGaAsBi detectors with different doping concentrations of InGaAsBi layers. The dark current characteristics are simulated at 300 K. The thickness of InGaAsBi is 1.5 μm. The doping concentration of InAlAs is 1×10^{18} cm^{-3}

图8 InGaAsBi探测器(a)暗电流-电压曲线,(b) -10 mV偏压下,总暗电流、扩散电流和产生复合电流随InGaAsBi掺杂浓度的变化曲线,其中,InGaAsBi的厚度为1.5 μm,InAlAs的掺杂浓度为1×10^{18} cm^{-3}

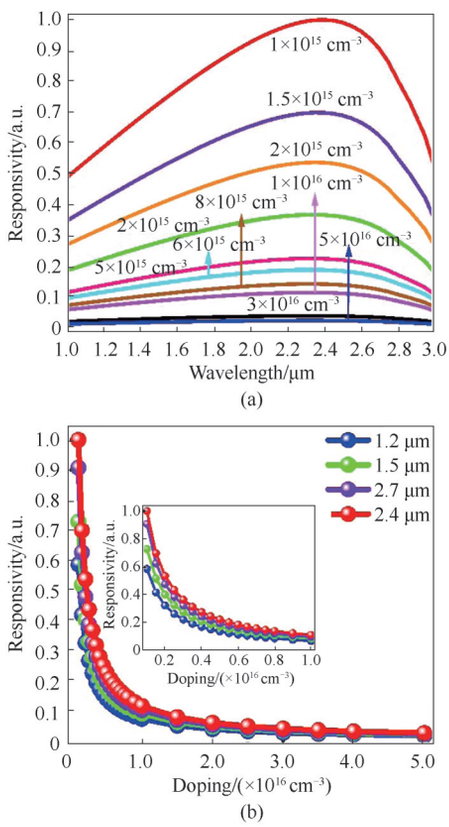

Fig. 9 Normalized responsivity spectra (a) and responsivities under different incident wavelengths (b) with different doping concentrations of InGaAsBi. The responsivities are calculated under a bias of -10 mV at 300 K. The thickness of InGaAsBi is 1.5 μm. The doping concentration of InAlAs is 1×10^{18} cm^{-3}

图9 不同InGaAsBi掺杂浓度下,InGaAsBi探测器:(a)归一化响应谱,(b)不同入射光波长下响应率随InGaAsBi掺杂浓度的变化曲线,其中,InGaAsBi的厚度为1.5 μm,InAlAs的掺杂浓度为1×10^{18} cm^{-3},拟合温度为300 K,偏置电压为-10 mV

strates [J]. *Journal of Applied Physics*, 1996. **79**(11): 8367-8370.
[7] Tian Z B, Gu Y, Wang K, *et al*. Gas source MBE-grown metamorphic InGaAs photodetectors using InAlAs buffer and cap layers with cut-off wavelength up to 2.7 μm [J]. *Chinese Physics Letters*, 2008. **25**(6):2292-2295.
[8] Du B, Gu Y, Chen X Y, *et al*. Improved performance of high indium InGaAs photodetectors with InAlAs barrier [J]. *Japanese Journal of Applied Physics*, 2018. **57**(6).
[9] Oe K. Characteristics of semiconductor alloy $GaAs_{1-x}Bi_x$ [J]. *Japanese Journal of Applied Physics*, 2002. **41**(Part 1, No. 5A): 2801-2806.
[10] Lu X F, Beaton D A, Lewis R B, *et al*. Composition dependence of photoluminescence of $GaAs_{1-x}Bi_x$ alloys [J]. *Applied Physics Letters*, 2009. **95**(4).
[11] Richards, R D, Bastiman F, Walker D, *et al*. Growth and structural characterization of GaAsBi/GaAs multiple quantum wells [J]. *Semiconductor Science and Technology*, 2015. **30**(9).
[12] Gu Y, Zhang Y G, Chen X Y, *et al*. Nearly lattice-matched short-wave infrared InGaAsBi detectors on InP [J]. *Applied Physic Letters*, 2016.108.
[13] Gu Y, Zhang Y G, Song Y X, *et al*. Optical properties of InGaAsBi/GaAs strained quantum wells studied by temperature-dependent photoluminescence [J]. *Chinese Physics B*, 2013, **22**:037802.
[14] Carrier P, Wei S H. Calculated spin-orbit splitting of all diamond-like and zinc-blende semiconductors: Effects of $p_{1/2}$ local orbitals and chemical trends [J]. *Physical Review B*, 2004. **70**(3).
[15] Zhou S X, Qi M, Ai L K, *et al*. Growth and electrical properties of high-quality InGaAsBi thin films using gas source molecular beam epitaxy [J]. *Japanese Journal of Applied Physics*, 2017, 56.
[16] Chen X Y, Gu Y, Zhang Y G, *et al*. Characteristics of InGaAsBi with various lattice mismatches on InP substrate [J]. *AIP Advances*, 2016. 6.
[17] Butkutė R, Pačebutas V, Čechavičius B, *et al*. Photoluminescence at up to 2.4μm wavelengths from GaInAsBi/AlInAs quantum wells [J]. *Journal of Crystal Growth*, 2014. **391**:116-120.
[18] Du B, G Y, Zhang Y G, *et al*. Wavelength extended InGaAsBi detectors with temperature-insensitive cutoff wavelength[J]. *Chinese Physics Letters*, 2018, **35**(7):078501.
[19] Paebutas V, Echaviius B, Krotkus A. Single quantum well diodes from GaInAsBi emitting at wavelengths up to 2.5 μm [J]. *Infrared Physics & Technology*, 2020.
[20] Jensen K M, R. Morgan, Murray R. B. Semiconductors and Semimetals[J]. *IOP sinence 1976 Phys. Bull*. 27 506.
[21] Yang Q K, Fuchs F, Schmitz J, *et al*. Investigation of trap-assisted tunneling current in InAs/(GaIn) Sb superlattice long-wavelength photodiodes [J]. *Applied Physics Letters*, 2002. **81**(25): 4757-4759.
[22] Wong J Y. Effect of trap tunneling on the performance of long-wavelength $Hg_{1-x}Cd_xTe$ photodiodes [J]. *Electron Devices*, IEEE Transactions on, 1980, **27**(1):48-57.
[23] Kinch M A. Electronic properties of HgCdTe [J]. *Journal of Vacuum*

Science and Technology, 1982. **21**(1): 215-219.
[24] Chen B, Yuan J R, A L Holmes. Dark current modeling of InP based SWIR and MWIR InGaAs/GaAsSb type-II MQW photodiodes. *Optical and Quantum Electronics*, 2013. **45**(3): p. 271-277.
[25] Galiev G B, Evskii I V, Klimov E A, *et al*. Specific features of the photoluminescence of HEMT nanoheterostructures containing a composite InAlAs/InGaAs/InAs/InGaAs/InAlAs quantum well [J]. *Semiconductors*, 2015, **49**(2): 234-241.
[26] Satzke K, Weiser G, Stolz W, *et al*. Optical study of the electronic states of $In_{0.53}Ga_{0.47}As$ /$In_{0.52}Al_{0.48}As$ quantum wells in high electric fields[J]. *Physical Review B*, 1991.
[27] Datta S, Shi S, Roenker K P, *et al*. Simulation and design of InAlAs/InGaAs p-n-p heterojunction bipolar transistors [J]. *IEEE Transactions on Electron Devices Ed*, 1998, **45**(8): 1634-1643.
[28] Sfina N, Ammar I, Lazzari J L, *et al*. Modelization of electrical and optical characteristics of short-wave infrared type I InGaAsBi/InGaAs/InP quantum wells p-i-n detector [J]. *Physica Scripta*, 2021, **96**(3): 035802 .
[29] ZHAO Xu. Structure optimization design of extended wavelength $In_{0.82}Ga_{0.18}As$ infrared detector device [J]. Graduate University of Chinese Academy of Sciences (Changchun Institute of Optics, Fine Mechanics and Physics), 2014.(赵旭. 延伸波长 $In_{0.82}Ga_{0.18}As$ 红外探测器器件结构优化设计[J]. 中国科学院研究生院(长春光学精密机械与物理研究所)), 2014.
[30] HU Wei- Da, YIN Fei, YE Zhen- Hua, *et al*. Effects of absorption layer characteristics and interfacial charges of heterojunction on the responsivity of 12.5μm long-wave HgCdTe photovoltaic detectors [J]. Acta Physics Sinica, 2009(11): 6.(胡伟达, 殷菲, 叶振华, 等. 吸收层特性和异质结界面电荷对12.5μm长波HgCdTe光伏探测器响应率的影响研究[J]. **物理学报**), 2009(11): 6.
[31] Ariyawansa G, Grupen M, Duran J M, *et al*. Design and modeling of InAs/GaSb type II superlattice based dual-band infrared detectors [J]. *Journal of Applied Physics*, 2012, **111**(7): 3498.